



HAL
open science

Finite-Frequency Noise and Dynamical Charge Susceptibility in Single and Double Quantum Dot Systems

Samuel Richard, Mireille Lavagna, Adeline Crépieux

► **To cite this version:**

Samuel Richard, Mireille Lavagna, Adeline Crépieux. Finite-Frequency Noise and Dynamical Charge Susceptibility in Single and Double Quantum Dot Systems. *Annalen der Physik*, 2023, 10.1002/andp.202300345 . hal-04324698

HAL Id: hal-04324698

<https://hal.science/hal-04324698v1>

Submitted on 1 Feb 2024

HAL is a multi-disciplinary open access archive for the deposit and dissemination of scientific research documents, whether they are published or not. The documents may come from teaching and research institutions in France or abroad, or from public or private research centers.

L'archive ouverte pluridisciplinaire **HAL**, est destinée au dépôt et à la diffusion de documents scientifiques de niveau recherche, publiés ou non, émanant des établissements d'enseignement et de recherche français ou étrangers, des laboratoires publics ou privés.

Finite-Frequency Noise and Dynamical Charge Susceptibility in Single and Double Quantum Dot Systems

Samuel Richard, Mireille Lavagna, and Adeline Crépieux*

This study reports on finite-frequency noise and dynamical charge susceptibility in out-of-equilibrium quantum dot systems. Both single and double quantum dots connected to one or two reservoirs of electrons are considered, and these quantities are calculated by using the non-equilibrium Green function technique. The results are discussed in the light of experimental results, particularly in the low-frequency limit for which an interpretation in terms of an equivalent RC-circuit is made. Anti-symmetrized noise is also studied, defined as the difference between absorption and emission noises, and its relationship with the dynamical charge susceptibility in single quantum dots is established. In double quantum dots, the similarities between the dynamical charge susceptibility, the absorption noise, and the dot occupancy, are highlighted by comparing their respective variations with the bias voltage applied between the two reservoirs, and the detuning energy defined as the difference between the lowest level energies in the two dots.

1. Introduction

In order to optimize the performance of quantum electronic circuits, such as qubits, it is of prime importance to understand how electromagnetic radiations, emitted by either an artificial or a natural source, affect the state and the phase coherence of the circuits.^[1–3] To achieve this goal, it is necessary to explore the relationship between the circuit sensitivity, i.e., its charge susceptibility, and the surrounding fluctuations, i.e., the electrical current noise. In a previous work,^[4] the relationship between the ac-conductance and the finite-frequency noise in a

quantum dot was established. However, ac-conductance does not inform us directly on the variation of dot occupancy, as charge susceptibility precisely does, since this latter quantity is related to the derivative of the dot occupancy with respect to the dot level energy. It is therefore necessary to focus on charge susceptibility rather than on ac-conductance.

There are a number of theoretical studies devoted either to dot occupancy,^[5–7] to charge susceptibility,^[8–10] or to electrical current noise^[11–19] in quantum dots, but none to the three quantities simultaneously. This work remedies this lack by studying these quantities together, first in a single quantum dot (SQD), and then in a double quantum dot (DQD), considering various geometrical arrangements for the dots. The aim is to examine

whether dot occupancy, dynamical charge susceptibility and finite-frequency noise in these systems present some common characteristics in their variation profile as a function of bias voltage or frequency, and if it is the case, to identify in what specific way.

On the experimental side, studies on charge susceptibility have been multiplying in recent years, in particular in DQD systems.^[20–22] As far as noise measurements are concerned, results are now available for both SDQ systems^[23–25] and QDQ systems.^[26–29] They show that the emission noise, i.e. the noise at positive frequency, is reduced to zero as soon as bias voltage applied to the circuit is lower than the frequency, and provide us with information on charge transfer, especially in the low-frequency limit, where the quantum dot system can be described as an equivalent RC-circuit.

The article is organized as follows. In Section 2, we present the Hamiltonian used to model the system, and we give the formal expressions for finite-frequency noise, dynamical charge susceptibility and dot occupancy. In Section 3, we study SQD systems specifically, looking at the exact relation between the anti-symmetrized noise and the charge susceptibility and exploring the low-frequency limit, while in Section 4 we discuss the numerical results obtained for DQD systems. We conclude in Section 5.

S. Richard, A. Crépieux
Aix Marseille Univ
Université de Toulon, CNRS, CPT
Marseille France
E-mail: adeline.crepieux@cpt.univ-mrs.fr

M. Lavagna
Univ. Grenoble Alpes, CEA, IRIG, PHELIQS
Grenoble F-38000, France

M. Lavagna
Centre National de la Recherche Scientifique, CNRS
Grenoble 38042, France

 The ORCID identification number(s) for the author(s) of this article can be found under <https://doi.org/10.1002/andp.202300345>

© 2023 The Authors. Annalen der Physik published by Wiley-VCH GmbH. This is an open access article under the terms of the Creative Commons Attribution-NonCommercial-NoDerivs License, which permits use and distribution in any medium, provided the original work is properly cited, the use is non-commercial and no modifications or adaptations are made.

DOI: 10.1002/andp.202300345

2. Model

2.1. Hamiltonian

To model SQD and DQD systems, we use the following Hamiltonian

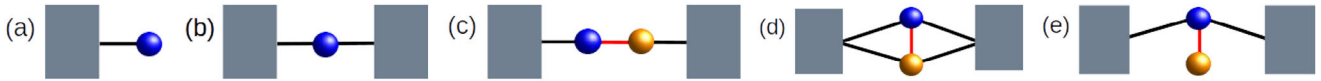


Figure 1. Schematic representation of the studied geometries: a) left-connected SQD, b) double-connected SQD, c) serial-coupled DQD, d) parallel-coupled DQD, and e) side-coupled DQD. The black lines denote the dot-reservoir coupling $\Gamma_{\alpha,ij}$, while the red lines represent the dot-dot coupling \mathcal{V}_{12} . The blue and yellow sphere represent dots 1 and 2, and the grey blocks the reservoirs.

$$\hat{H} = \sum_{\substack{\alpha=L,R \\ k \in \alpha}} \varepsilon_{ak} \hat{c}_{ak}^\dagger \hat{c}_{ak} + \sum_{\substack{i=1,2 \\ n \in i}} \varepsilon_{in} \hat{a}_{in}^\dagger \hat{a}_{in} + \sum_{\substack{n \in 1 \\ m \in 2}} \mathcal{V}_{12} \hat{a}_{2m}^\dagger \hat{a}_{1n} + \sum_{\substack{\alpha=L,R \\ k \in \alpha}} \sum_{\substack{i=1,2 \\ n \in i}} V_{i\alpha} \hat{c}_{ak}^\dagger \hat{a}_{in} + h.c. \quad (1)$$

where \hat{c}_{ak}^\dagger (\hat{c}_{ak}) is the creation (annihilation) electron operator in reservoir α , with momentum k and energy ε_{ak} , and \hat{a}_{in}^\dagger (\hat{a}_{in}) is the creation (annihilation) electron operator in dot i , with $i = 1, 2$ and energy level n , with $n \in [0, N - 1]$ where N is the number of energy levels in the dot i . The notation *h.c.* denotes the hermitian conjugate terms associated with the third and fourth contributions in Equation (1). One assumes that the hopping integral $V_{i\alpha}$ between the states $|in\rangle$ in the dot i and $|ak\rangle$ in the reservoir α does not depend on momentum k or index n . By using the Hamiltonian of Equation (1), one can model several geometries for the quantum dot system, such as left-connected or double-connected SQD, and serial-coupled, parallel-coupled, or side-coupled DQD, as depicted in **Figure 1**, the study of the latter geometry being in expansion.^[30–32] To do this, we simply play with the values taken by the dot-reservoir coupling $\Gamma_{\alpha,ij}$ and the dot-dot coupling \mathcal{V}_{12} , as summarized in **Table 1**. These quantum dot systems are driven in an out-of-equilibrium situation under the application of a bias voltage defined as $V = \mu_L - \mu_R$, where μ_L and μ_R are the chemical potentials of the left and right reservoirs. Gate voltages V_{gi} are also applied in such systems, determining the position of the energy levels ε_{in} in each of the dots.

2.2. Dynamical Charge Susceptibility and Dot Occupancy

For quantum dots submitted to dc voltage, the dynamical charge susceptibility $\chi(\omega)$ is given by the Fourier transform of the quantity $\chi(t, t')$ defined as the average value of the commutator between operators $\Delta \hat{N}_i(t)$, where $\Delta \hat{N}_i(t) = \hat{N}_i(t) - \langle \hat{N}_i \rangle$. Indeed, one has $\chi(t, t') = i\Theta(t - t') \langle [\Delta \hat{N}_1(t), \Delta \hat{N}_1(t')] \rangle$ for SQD, and $\chi(t, t') = i\Theta(t - t') \sum_{i,j=1,2} \beta_i \beta_j \langle [\Delta \hat{N}_i(t), \Delta \hat{N}_j(t')] \rangle$ for DQD,

Table 1. Values taken by the dot-reservoir coupling $\Gamma_{\alpha,ij}$ and dot-dot coupling \mathcal{V}_{12} for the various studied geometries.

Left-connected SQD	Double-connected SQD	Serial-coupled DQD	Parallel-coupled DQD	Side-coupled DQD
$\Gamma_{L,11} = \Gamma_L$	$\Gamma_{L,11} = \Gamma_L$	$\Gamma_{L,11} = \Gamma$	$\Gamma_{L,11} = \Gamma$	$\Gamma_{L,11} = \Gamma$
$\Gamma_{L,22} = 0$	$\Gamma_{L,22} = 0$	$\Gamma_{L,22} = 0$	$\Gamma_{L,22} = \Gamma$	$\Gamma_{L,22} = \Gamma$
$\Gamma_{R,11} = 0$	$\Gamma_{R,11} = \Gamma_R$	$\Gamma_{R,11} = 0$	$\Gamma_{R,11} = \Gamma$	$\Gamma_{R,11} = 0$
$\Gamma_{R,22} = 0$	$\Gamma_{R,22} = 0$	$\Gamma_{R,22} = \Gamma$	$\Gamma_{R,22} = \Gamma$	$\Gamma_{R,22} = 0$
$\mathcal{V}_{12} = 0$	$\mathcal{V}_{12} = 0$	$\mathcal{V}_{12} = \mathcal{V}$	$\mathcal{V}_{12} = \mathcal{V}$	$\mathcal{V}_{12} = \mathcal{V}$

where Θ is the Heaviside function, $\hat{N}_i = \sum_{n \in i} \hat{a}_{in}^\dagger \hat{a}_{in}$ is the operator associated with the number of electrons in the dot i , and $\beta_{1,2}$ is the lever-arm coefficient measuring the asymmetry of the capacitive couplings of each of the two dots to the gate voltage.^[33] In the following, we assume symmetrical capacitive coupling, meaning that $\beta_{1,2} = 1$. The dynamical charge susceptibility for the systems we consider can be calculated by using the technique of non-equilibrium Green functions.^[34] We obtain the following expression

$$\chi(\omega) = i \int_{-\infty}^{\infty} \frac{d\varepsilon}{2\pi} \text{Tr} \left\{ \underline{\underline{\mathbf{G}}}^<(\varepsilon) \left[\underline{\underline{\mathbf{G}}}^a(\varepsilon - \hbar\omega) + \underline{\underline{\mathbf{G}}}^r(\varepsilon + \hbar\omega) \right] \right\} \quad (2)$$

where $\underline{\underline{\mathbf{G}}}^<$, $\underline{\underline{\mathbf{G}}}^r$, $\underline{\underline{\mathbf{G}}}^a$ are the lesser, retarded, and advanced Green functions, respectively. The retarded/advanced Green functions 2×2 matrices are given by

$$\underline{\underline{\mathbf{G}}}^{r/a}(\varepsilon) = \frac{1}{D^{r/a}(\varepsilon)} \begin{pmatrix} \tilde{\mathbf{g}}_1^{r/a}(\varepsilon) & \tilde{\mathbf{g}}_1^{r/a}(\varepsilon) \tilde{\Sigma}_{12}^{r/a}(\varepsilon) \tilde{\mathbf{g}}_2^{r/a}(\varepsilon) \\ \tilde{\mathbf{g}}_2^{r/a}(\varepsilon) \tilde{\Sigma}_{21}^{r/a}(\varepsilon) \tilde{\mathbf{g}}_1^{r/a}(\varepsilon) & \tilde{\mathbf{g}}_2^{r/a}(\varepsilon) \end{pmatrix} \quad (3)$$

with $D^{r/a}(\varepsilon) = 1 - \tilde{\mathbf{g}}_1^{r/a}(\varepsilon) \tilde{\Sigma}_{12}^{r/a}(\varepsilon) \tilde{\mathbf{g}}_2^{r/a}(\varepsilon) \tilde{\Sigma}_{21}^{r/a}(\varepsilon)$ and $\tilde{\mathbf{g}}_i^{r/a}(\varepsilon) = \mathbf{g}_i^{r/a}(\varepsilon) / (1 - \tilde{\Sigma}_{ii}^{r/a}(\varepsilon) \mathbf{g}_i^{r/a}(\varepsilon))$. In these expressions, it appears the retarded Green function of the disconnected dot i , defined as $\mathbf{g}_i^{r/a}(\varepsilon) = \sum_{n \in i} \mathbf{g}_{in}^{r/a}(\varepsilon)$ where $\mathbf{g}_{in}^{r/a}(\varepsilon) = 1 / (\varepsilon - \varepsilon_{in} \pm i0^+)$ with $\varepsilon_{in} = \varepsilon_i + n\varepsilon_0$, and the total self-energy: $\tilde{\Sigma}^{r/a}(\varepsilon) = \sum_{\alpha=L,R} \underline{\underline{\Sigma}}_{\alpha}^{r/a}(\varepsilon) + \underline{\underline{\Sigma}}_{\text{int}}^{r/a}$, where the matrix $\underline{\underline{\Sigma}}_{\text{int}}^{r/a}$ is given by

$$\underline{\underline{\Sigma}}_{\text{int}}^r = \begin{pmatrix} 0 & \mathcal{V}_{12}^* \\ \mathcal{V}_{21}^* & 0 \end{pmatrix} \quad \text{and} \quad \underline{\underline{\Sigma}}_{\text{int}}^a = \begin{pmatrix} 0 & \mathcal{V}_{12} \\ \mathcal{V}_{21} & 0 \end{pmatrix} \quad (4)$$

The self-energy matrices associated with the reservoir α are given by $\underline{\underline{\Sigma}}_{\alpha}^{r/a}(\varepsilon) = \mp(i/2)\Gamma_{\alpha}$, $\underline{\underline{\Sigma}}_{\alpha}^<(\varepsilon) = if_{\alpha}^e(\varepsilon)\Gamma_{\alpha}$ and $\underline{\underline{\Sigma}}_{\alpha}^>(\varepsilon) = -if_{\alpha}^h(\varepsilon)\Gamma_{\alpha}$, where $f_{\alpha}^e(\varepsilon) = 1 / (1 + \exp(\varepsilon - \mu_{\alpha}) / k_B T_{\alpha})$ is the Fermi-Dirac distribution functions with T_{α} the temperature and μ_{α} the chemical potential of the reservoir α , and $f_{\alpha}^h(\varepsilon) = 1 - f_{\alpha}^e(\varepsilon)$. We define the elements of the dot-reservoir coupling matrix $\underline{\underline{\Gamma}}_{\alpha}$ as $\Gamma_{\alpha,ij} = 2\pi \rho_{\alpha} V_{i\alpha}^* V_{j\alpha}$, where the density of states ρ_{α} in the reservoir α is assumed to be energy independent in the wide-band limit. By using the relation $\underline{\underline{\mathbf{G}}}^<(\varepsilon) = \sum_{\alpha=L,R} \underline{\underline{\mathbf{G}}}^r(\varepsilon) \underline{\underline{\Sigma}}_{\alpha}^<(\varepsilon) \underline{\underline{\mathbf{G}}}^a(\varepsilon)$, and by introducing the charge susceptibility associated with the left reservoir, $\chi_L(\omega)$, through the relation $\chi(\omega) = \chi_L(\omega) + \chi_R(\omega)$, one gets

$$\chi_L(\omega) = - \int_{-\infty}^{\infty} \frac{d\varepsilon}{2\pi} f_L^e(\varepsilon) \times \text{Tr} \left\{ \underline{\underline{\mathbf{G}}}^r(\varepsilon) \underline{\underline{\Gamma}}_L \underline{\underline{\mathbf{G}}}^a(\varepsilon) \left[\underline{\underline{\mathbf{G}}}^a(\varepsilon - \hbar\omega) + \underline{\underline{\mathbf{G}}}^r(\varepsilon + \hbar\omega) \right] \right\} \quad (5)$$

The electron occupancy in the dot i is given by the average value of the operator $\widehat{\mathcal{N}}_i$. It is equal to

$$\langle \widehat{\mathcal{N}}_i \rangle = -i \int_{-\infty}^{\infty} \frac{d\varepsilon}{2\pi} \mathbf{G}_{ii}^<(\varepsilon) \quad (6)$$

The sum over the dot index i , of the derivatives of the dot occupancy with respect to the dot level energies, gives the charge susceptibility at zero frequency, i.e., the static charge susceptibility $\chi(\omega = 0)$. Indeed, one has the equality

$$\frac{\partial \mathbf{G}_{ij}^{r/a}(\varepsilon)}{\partial \varepsilon_j} = \mathbf{G}_{ij}^{r/a}(\varepsilon) \mathbf{G}_{ji}^{r/a}(\varepsilon) \quad (7)$$

which leads to the relation $\partial \langle \widehat{\mathcal{N}}_i \rangle / \partial \varepsilon_j = -i \int_{-\infty}^{\infty} [\mathbf{G}_{ij}^<(\varepsilon) \mathbf{G}_{ji}^>(\varepsilon) + \mathbf{G}_{ij}^>(\varepsilon) \mathbf{G}_{ji}^<(\varepsilon)] d\varepsilon$. Next, by setting $\omega = 0$ in Equation (2), one shows that $\chi(\omega = 0)$ is related to the sum of the derivatives of dot occupancies with respect to dot level energies through the relation

$$\chi(\omega = 0) = - \sum_{ij} \frac{\partial \langle \widehat{\mathcal{N}}_i \rangle}{\partial \varepsilon_j} \quad (8)$$

Generally speaking, the expression of the static charge susceptibility given by Equation (8) can also be derived from the definition of the dynamical charge susceptibility $\chi(\omega) = \lim_{\Delta V_g(\omega) \rightarrow 0} \sum_{i=1,2} d \langle \widehat{\mathcal{N}}_i \rangle / d \Delta \varepsilon V_g(\omega)$.^[33]

2.3. Finite-Frequency Noise and Anti-Symmetized Noise

The finite-frequency noise $S_{\alpha\alpha'}(\omega)$ is defined as the Fourier transform of the current-current correlator: $S_{\alpha\alpha'}(t, t') = \langle \Delta \widehat{I}_\alpha(t) \Delta \widehat{I}_{\alpha'}(t') \rangle$, where $\Delta \widehat{I}_\alpha(t) = \widehat{I}_\alpha(t) - \langle \widehat{I}_\alpha(t) \rangle$, with $\widehat{I}_\alpha = (ei/\hbar) \sum_{k \in \alpha, i=1,2, n \in i} (V_{ia} \widehat{c}_{ak}^\dagger \widehat{d}_{in} - V_{ia}^* \widehat{d}_{in}^\dagger \widehat{c}_{ak})$ the current operator associated with reservoir α . The finite-frequency noise associated with the left reservoir, i.e., when $\alpha = \alpha' = L$, can be calculated by using the non-equilibrium Green function technique.^[35–37] We obtain

$$\begin{aligned} S_{LL}(\omega) = & \frac{e^2}{h} \int_{-\infty}^{\infty} d\varepsilon \text{Tr} \left\{ f_R^e(\varepsilon) f_R^h(\varepsilon - \hbar\omega) \underline{\underline{\mathcal{T}}}_{RL}(\varepsilon) \underline{\underline{\mathcal{T}}}_{RL}(\varepsilon - \hbar\omega) \right. \\ & + f_L^e(\varepsilon) f_L^h(\varepsilon - \hbar\omega) \left[\underline{\underline{\mathcal{T}}}_{LL}^{\text{eff}}(\varepsilon) \underline{\underline{\mathcal{T}}}_{LL}^{\text{eff}}(\varepsilon - \hbar\omega) \right. \\ & + \left. \left(\underline{\underline{t}}_{LL}(\varepsilon) - \underline{\underline{t}}_{LL}(\varepsilon - \hbar\omega) \right) \left(\underline{\underline{t}}_{LL}^+(\varepsilon) - \underline{\underline{t}}_{LL}^+(\varepsilon - \hbar\omega) \right) \right] \\ & + f_L^e(\varepsilon) f_R^h(\varepsilon - \hbar\omega) \left[1 - \underline{\underline{\mathcal{T}}}_{LL}^{\text{eff}}(\varepsilon) \right] \underline{\underline{\mathcal{T}}}_{RL}(\varepsilon - \hbar\omega) \\ & \left. + f_R^e(\varepsilon) f_L^h(\varepsilon - \hbar\omega) \underline{\underline{\mathcal{T}}}_{RL}(\varepsilon) \left[1 - \underline{\underline{\mathcal{T}}}_{LL}^{\text{eff}}(\varepsilon - \hbar\omega) \right] \right\} \quad (9) \end{aligned}$$

where $\underline{\underline{t}}_{\alpha\alpha}(\varepsilon) = i \underline{\underline{\mathbf{G}}}^r(\varepsilon) \underline{\underline{\Gamma}}_\alpha$ is the transmission amplitude, $\underline{\underline{\mathcal{T}}}_{\alpha\beta}(\varepsilon) = \underline{\underline{\mathbf{G}}}^r(\varepsilon) \underline{\underline{\Gamma}}_\alpha \underline{\underline{\mathbf{G}}}^a(\varepsilon) \underline{\underline{\Gamma}}_\beta$ is the transmission coefficient, and $\underline{\underline{\mathcal{T}}}_{\alpha\alpha}^{\text{eff}}(\varepsilon) =$

$\underline{\underline{t}}_{\alpha\alpha}(\varepsilon) + \underline{\underline{t}}_{\alpha\alpha}^+(\varepsilon) - \underline{\underline{\mathcal{T}}}_{\alpha\alpha}(\varepsilon)$. At positive frequencies, $S_{LL}(\omega)$ corresponds to the emission noise whereas at negative frequencies, it corresponds to the absorption noise.^[11,23,24] The anti-symmetized noise, introduced in order to compare dynamical charge susceptibility and finite-frequency noise, is defined as the difference between absorption noise and emission noise, according to

$$A_L(\omega) = S_{LL}(-\omega) - S_{LL}(\omega) \quad (10)$$

3. Results and Discussion for SQD Systems

3.1. Evolution of Charge Susceptibility and Noise with Bias Voltage

We start our discussion by considering a double-connected SQD (see Figure 1b), focusing on charge susceptibility and noise associated with the left reservoir, namely $\chi_L(\omega)$ and $S_{LL}(\omega)$ given by Equations (5) and (9), respectively. In **Figure 2** these two quantities are plotted as a function of the bias voltage V for both single-level ($N = 1$) and multi-level ($N = 3$) dot. With regard to noise, one observes three main features when one compares the emission noise $S_{LL}(\omega > 0)$, depicted by solid lines, and the absorption noise $S_{LL}(\omega < 0)$, depicted by dashed lines: i) over the entire bias voltage range, the values taken by the absorption noise are greater than, or equal to those taken by the emission noise $S_{LL}(\omega > 0)$; ii) the emission and absorption noises strongly differ at low voltage with the reduced to zero emission noise at $eV < |\hbar\omega|$, while the absorption noise is non-zero in that regime; and iii) at higher voltage, i.e., for $eV > |\hbar\omega|$, the emission and absorption noises converge to an identical value, which may depend on frequency. As far as the charge susceptibility is concerned, a remarkable result is obtained when there is more than one energy level in the dot. Indeed, in that case, the quantity $|\chi_L(\omega)|$ at low voltage may take high value at finite frequency (see the green curve in the $N = 3$ panel) in a regime where the emission noise is reduced to zero, meaning that one could quite easily vary the dot occupancy in the SQD in that operating regime without significant noise pollution. Moreover, the charge susceptibility at low voltage is more stable at finite frequency than at zero frequency (compare the red and green curves in the $N = 3$ panel), allowing finer control of the dot occupancy.

The noise and charge susceptibility in a left-connected SQD (see Figure 1a) are plotted in **Figure 3**. The main difference with the results obtained for the double-connected SQD relies on the fact that the emission noise is reduced to zero in a left-connected SQD, since $\Gamma_R = 0$, while it is non-zero in a double-connected SQD. We can thus conclude that there is no emission noise for such a system, at least at low temperature, i.e., when $k_B T$ is small compared to the dot-reservoir coupling Γ_L . Note that this will be no longer true at temperature larger or of the order of the dot-reservoir coupling. We also note that the absorption noise is reduced to zero for $eV > |\hbar\omega|$, which did not occur in the case of a double-connected SQD. This can therefore be seen as a particular feature of left-connected SQD. For the sake of completeness, we should point out that in the presence of Coulomb interactions, emission noise would become non-zero at $eV < \hbar\omega$ due to the presence of inelastic tunneling processes.^[38,39]

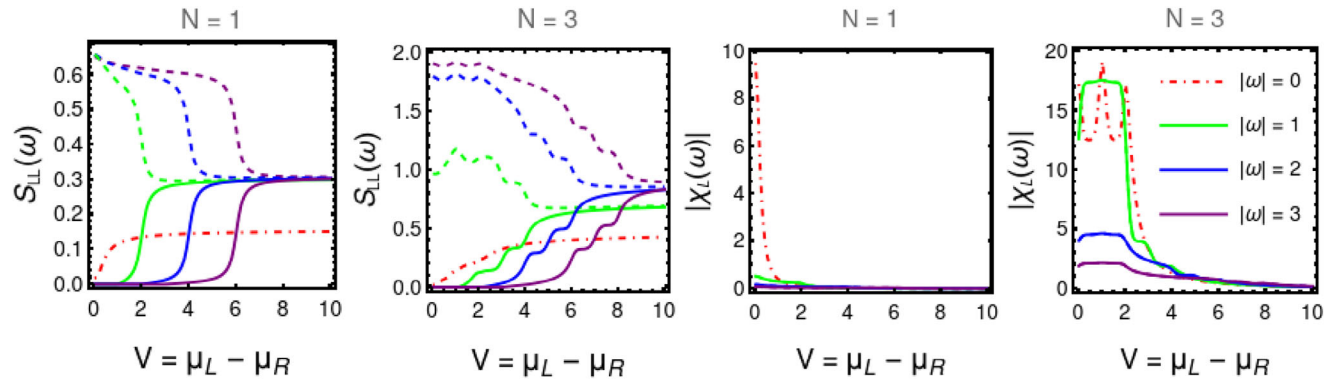


Figure 2. Noise and dynamical charge susceptibility in a double-connected SQD as a function of bias voltage V , for various values of frequency ω at $\Gamma_{L,R} = 0.1$, $\varepsilon_1 = 0$, $\varepsilon_0 = 0.5$, and $T = 0.01$ for both one energy level ($N = 1$) and three energy levels ($N = 3$) in the dot. The solid, dashed and dotted-dashed lines in the $S_{LL}(\omega)$ plots correspond to the emission ($\omega > 0$), absorption ($\omega < 0$) and zero-frequency noise, respectively. One has $|\chi_L(-\omega)| = |\chi_L(\omega)|$.

3.2. Relationship Between Anti-Symmetrized Noise and Dynamical Charge Susceptibility

When $N = 1$, there exists an exact relationship between the anti-symmetrized noise and the dynamical charge susceptibility in the left reservoir for SQD systems. Indeed, in that case, Equation (10) can be rewritten as

$$\chi_L(\omega) = -\frac{i}{\Gamma_L \Gamma_R} \int_{-\infty}^{\infty} \frac{d\varepsilon}{2\pi} \left[f_L^e(\varepsilon - \hbar\omega) \mathcal{T}_{LR}(\varepsilon - \hbar\omega) t_{LL}(\varepsilon) - f_L^e(\varepsilon) \mathcal{T}_{LR}(\varepsilon) t_{LL}^*(\varepsilon - \hbar\omega) \right] \quad (11)$$

since the Green functions and transmission coefficients and amplitudes are no longer matrices. Moreover, by inserting Equation (9) in Equation (10), one gets after simplification

$$\mathcal{A}_L(\omega) = \frac{e^2}{h} \int_{-\infty}^{\infty} d\varepsilon \left[f_L^e(\varepsilon - \hbar\omega) - f_L^e(\varepsilon) \right] \left[|t_{LL}(\varepsilon) - t_{LL}^*(\varepsilon - \hbar\omega)|^2 + \mathcal{T}_{LR}(\varepsilon) + \mathcal{T}_{LR}(\varepsilon - \hbar\omega) \right] \quad (12)$$

By using the relations between the transmission coefficient $\mathcal{T}_{LR}(\varepsilon)$ and the transmission amplitude $t_{LL}(\varepsilon)$, one establishes a relationship between the anti-symmetrized noise and the dynamical

charge susceptibility. For a double-connected SQD this relation reads

$$\mathcal{A}_L(\omega) = 2e^2 \omega \text{Im} \{ (\hbar\omega + i\Gamma_R) \chi_L(\omega) \} \quad (13)$$

whereas for a left-connected SQD, it reads

$$\mathcal{A}_L(\omega) = 2\hbar e^2 \omega^2 \text{Im} \{ \chi_L(\omega) \} \quad (14)$$

These results reveal the close connexion between finite-frequency noise and dynamical charge susceptibility in quantum dots. By explicitly calculating the dynamical charge susceptibility at zero temperature, starting from Equation (5), one gets for a double-connected SQD

$$\chi_L(\omega) = -\frac{\Gamma_L}{\hbar\omega(\hbar\omega + i(\Gamma_L + \Gamma_R))} \times \ln \left(1 - \frac{\hbar\omega(\hbar\omega + i(\Gamma_L + \Gamma_R))A(\mu_L)}{\Gamma_L + \Gamma_R} \right) \quad (15)$$

and for a left-connected SQD

$$\chi_L(\omega) = -\frac{\Gamma_L}{\hbar\omega(\hbar\omega + i\Gamma_L)} \ln \left(1 - \frac{\hbar\omega(\hbar\omega + i\Gamma_L)A(\mu_L)}{\Gamma_L} \right) \quad (16)$$

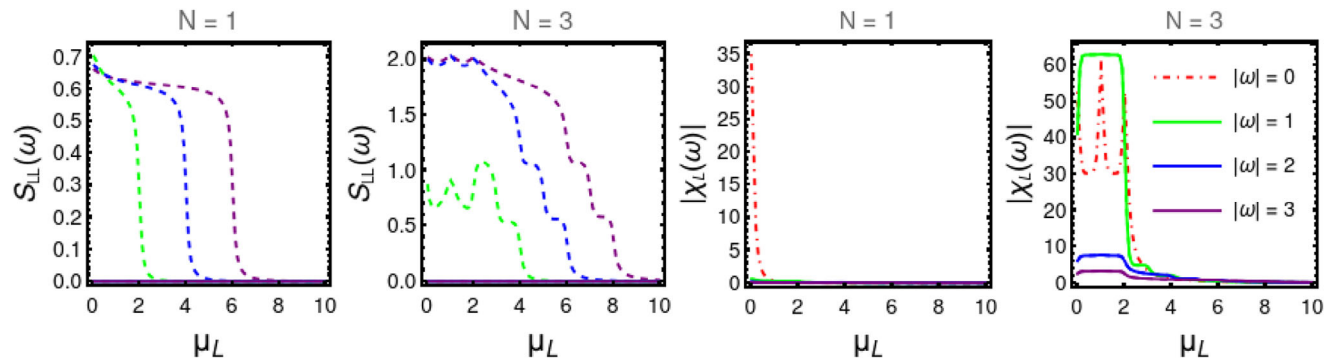


Figure 3. Noise and dynamical charge susceptibility in a left-connected SQD as a function of μ_L , the chemical potential of the left reservoir, for various values of frequency ω at $\Gamma_L = 0.1$ and $\Gamma_R = 0$. The other parameters are unchanged.

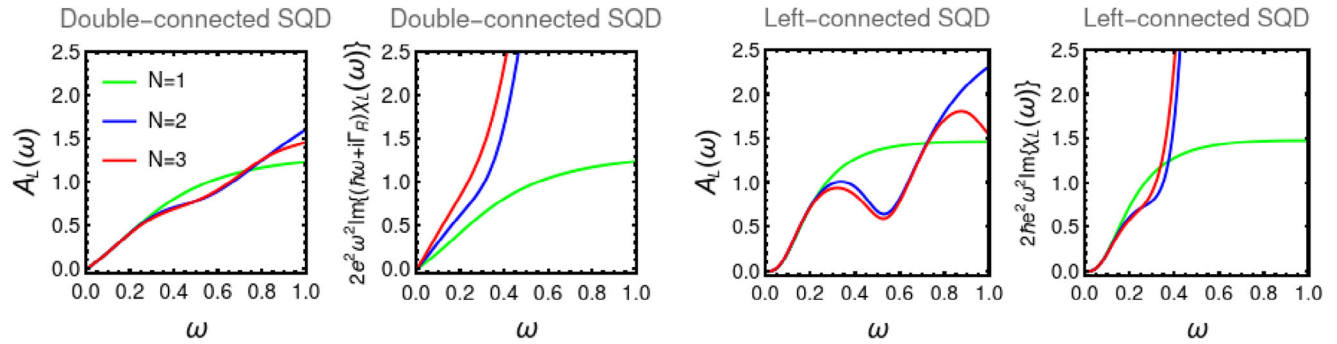


Figure 4. Anti-symmetrized noise in both double-connected and left-connected SQD systems at $V = 0$ and $T = 0.01$. One takes $\Gamma_{L,R} = 0.2$ for the double-connected SQD, and $\Gamma_L = 0.2$ and $\Gamma_R = 0$ for the left-connected SQD. For a comparison, we also plot the right-hand-side terms of Equations (13) and (14).

where $A(\mu_L)$ is the value taken by the spectral function at an energy equal to the chemical potential μ_L of the left reservoir. At low frequency compared to the dot-reservoirs couplings, it gives, up to the first order in ω , for a double-connected SQD

$$\chi_L(\omega) = \frac{A(\mu_L)\Gamma_L}{\Gamma_L + \Gamma_R} + i \frac{A^2(\mu_L)\Gamma_L}{2(\Gamma_L + \Gamma_R)} h\omega \quad (17)$$

and for a left-connected SQD

$$\chi_L(\omega) = A(\mu_L) + i \frac{A^2(\mu_L)}{2} h\omega \quad (18)$$

From these expressions, one can extract two results. First, one can deduce the effective capacitance C_L and resistance R_L of the equivalent RC-circuit associated with the left part of the SQD system. Second, one can explicitly express the anti-symmetrized noise at zero temperature and low frequency, as presented below.

3.2.1. Equivalent RC-circuit

The effective capacitance C_L and resistance R_L of the equivalent RC-circuit are given by $C_L = e^2 \chi_L(\omega = 0)$ and $R_L = (e/C_L)^2 \lim_{\omega \rightarrow 0} \text{Im}\{\chi_L(\omega)/\omega\}$.^[40,41] In a double-connected SQD, it leads to

$$C_L = \frac{e^2 A(\mu_L)\Gamma_L}{\Gamma_L + \Gamma_R} \xrightarrow{\Gamma_{L,R}=\Gamma} C_L = \frac{e^2 A(\mu_L)}{2} \quad \text{and} \quad R_L = \frac{h(\Gamma_L + \Gamma_R)}{2e^2\Gamma_L} \xrightarrow{\Gamma_{L,R}=\Gamma} R_L = \frac{h}{e^2} \quad (19)$$

and in a left-connected SQD to

$$C_L = e^2 A(\mu_L) \quad \text{and} \quad R_L = \frac{h}{2e^2} \quad (20)$$

In summary, one gets $R_L = R_Q$ for a double-connected SQD, and $R_L = R_Q/2$ for a left-connected SQD, where $R_Q = h/e^2$ is the quantum of resistance for spinless system. The fact that one obtains half of the quantum of resistance for a left-connected SQD was predicted theoretically^[42] and unambiguously demonstrated experimentally.^[43]

3.2.2. Anti-Symmetrized Noise in the Low-Frequency Limit

The anti-symmetrized noise at zero temperature and low frequency can be derived by incorporating Equations (17) and (18) into Equations (13) and (14). To the lowest order in ω , one obtains for a double-connected SQD

$$\mathcal{A}_L(\omega) = -\frac{2e^2\omega A(\mu_L)\Gamma_L\Gamma_R}{\Gamma_L + \Gamma_R} \quad (21)$$

and for a left-connected SQD

$$\mathcal{A}_L(\omega) = 2\pi e^2 \hbar^2 \omega^3 A^2(\mu_L) \quad (22)$$

Therefore, the dependency of the anti-symmetrized noise with frequency strongly differs between the left-connected and double-connected SQD systems. Indeed, at low frequency, $\mathcal{A}_L(\omega)$ varies linearly in ω in a double-connected SQD while its variation follows a power law of ω in a left-connected SQD, as can be seen in **Figure 4** where the results obtained from the exact expressions of $\mathcal{A}_L(\omega)$ given by Equations (9) and (10) are plotted as a function of ω . One can also see that Equations (13) and (14) hold for $N = 1$ only (see green curves in **Figure 4**). Indeed, when $N \neq 1$, the expressions given by Equations (13) and (14) linking $\mathcal{A}_L(\omega)$ to $\chi_L(\omega)$ no longer hold (see blue and red curves in **Figure 4**).

4. Results and Discussion for DQD Systems

In this section, we study noise and dynamical charge susceptibility in a DQD. We first consider a serial-coupled DQD, then a parallel-coupled DQD and finally a side-coupled DQD. Contrary to what we have shown for SQD systems through Equations (13) and (14), there is no simple relationship between emission noise, absorption noise and dynamical charge susceptibility for DQD. However one can identify similar behaviors between some of these quantities.

4.1. Serial-Coupled DQD

Figures 5 and **6** display the color-scale plots of the emission noise, absorption noise, dynamical charge susceptibility, and total dot

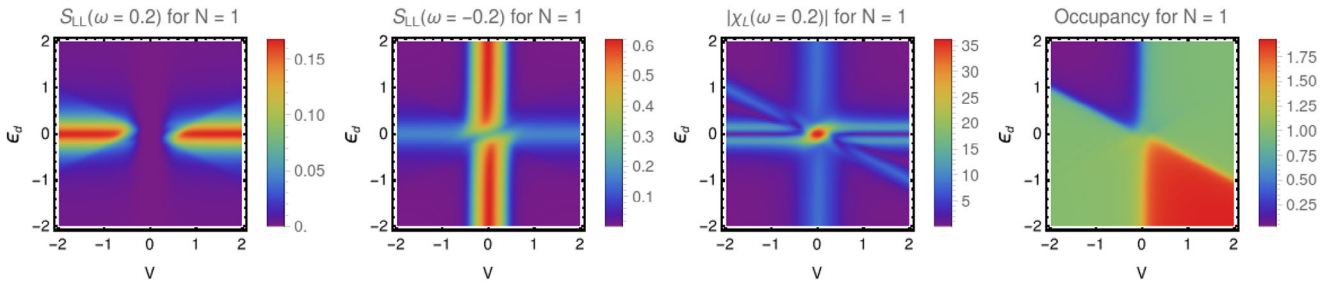


Figure 5. Color-scale plot for $S_{LL}(\omega)$, $|\chi_L(\omega)|$ and $\langle \hat{\mathcal{N}} \rangle$ in a serial-coupled DQD, as a function of bias voltage V and detuning energy ϵ_d at $|\omega| = 0.2$, $\Gamma_{L,R} = 0.1$, $\mathcal{V} = 0.1$, $\epsilon_1 = 0$, and $T = 0.01$, for one energy level in each dot ($N = 1$).

occupancy, $\langle \hat{\mathcal{N}} \rangle = \langle \hat{\mathcal{N}}_1 \rangle + \langle \hat{\mathcal{N}}_2 \rangle$ in a serial-coupled DQD, as depicted in Figure 1c. We first consider a single-level DQD with a single energy level per dot ($N = 1$) and we plot these latter quantities as a function of bias voltage V and detuning energy $\epsilon_d = \epsilon_2 - \epsilon_1$, two variables that can be experimentally varied. The first of the features observed in Figure 5 is the existence of a vertical central band around $V = 0$, whose width is equal to $2\hbar\omega/e$, within which the emission noise $S_{LL}(\omega > 0)$ is zero. This behavior is explained by the fact that, at low temperature, the system cannot emit energy at a voltage that is lower than the measurement frequency ω , here taken equal to 0.2 in arbitrary units. Within this interval, i.e., when $|eV| < \hbar\omega$, the module of the charge susceptibility, $|\chi_L(\omega)|$, is non-zero. Thus, as it is the case for a SQD, there is an operating regime where the charge susceptibility is high while the emission noise is zero. The second characteristic that can be observed is that absorption noise and charge susceptibility behave quite similarly, with the presence of two ridges in the plane (V, ϵ_d) , one vertical and one horizontal, forming a cross, within which $S_{LL}(\omega < 0)$ and $|\chi_L(\omega)|$ are non-zero. However, the charge susceptibility exhibits an additional narrow ridge along the line of equation $\epsilon_d = -eV/2$, which is directly related to the change in the dot occupancy $\langle \hat{\mathcal{N}} \rangle$ value, as can be seen in the right panel of Figure 5. The profile of $|\chi_L(\omega)|$ is thus a witness of both the behavior of the absorption noise and the dot occupancy.

We now turn our interest to the multi-level case where one has three energy levels per dot ($N = 3$). Figure 6 shows the presence of multiple ridges in the color-scale plot of the emission noise as a function of V and ϵ_d . However, the central band around $V = 0$ within which the emission noise $S_{LL}(\omega > 0)$ is zero is still present and its width is unchanged from the single-level case $N = 1$. There are also additional ridges in the absorption noise $S_{LL}(\omega < 0)$, which show a similar pattern to those of the emis-

sion noise $S_{LL}(\omega > 0)$ when $eV < -|\hbar\omega|$, while their patterns strongly differ when $eV > -|\hbar\omega|$. The charge susceptibility exhibits a complex variation profile since it is a mixing of the variations of the absorption noise and dot occupancy. For $N = 3$, the dot occupancy $\langle \hat{\mathcal{N}} \rangle$ exhibits seven plateaus (even if only six are visible in Figure 6), while for $N = 1$, it exhibits three plateaus (see Figure 5). This results from the Pauli exclusion principle, which requires $\langle \hat{\mathcal{N}} \rangle$ to take integer values in the interval $[0, 2N]$, leading to $\langle \hat{\mathcal{N}} \rangle \in [0, 2]$ for $N = 1$, and to $\langle \hat{\mathcal{N}} \rangle \in [0, 6]$ for $N = 3$.

4.2. Parallel-Coupled DQD

Figures 7 and 8 display $S_{LL}(\omega)$, $\chi_L(\omega)$ and $\langle \hat{\mathcal{N}} \rangle$ in a parallel-coupled DQD (see Figure 1d), as a function of bias voltage and detuning energy, with $N = 1$ and $N = 3$, respectively. The vertical band inside which the emission noise is zero is still there. Moreover, as it is the case for serial-coupled DQD, the variation profile of the charge susceptibility exhibits features, which are already present in the absorption noise variation profile and/or in the dot occupancy variation profile, and the plateaus in the dot occupancy are clearly visible in both the $N = 1$ and $N = 3$ cases. The main difference compared to what is obtained in the serial-coupled DQD, is the presence of a vertical symmetry axis, located at $V = 0$, in both the charge susceptibility and the dot occupancy variations. It results from the fact that in parallel-coupled DQD the bias profile across the DQD systems is unchanged under a sign inversion of V , while it is not the case in serial-coupled DQD. Beside, one observes the presence of horizontal lines located at the position $\epsilon_d = 0$ for $N = 1$, and at positions $\epsilon_d = -2\epsilon_0, -\epsilon_0, 0, \epsilon_0$ for $N = 3$. These positions correspond to the alignment of the energy levels of each of the two dots. There values can be obtained

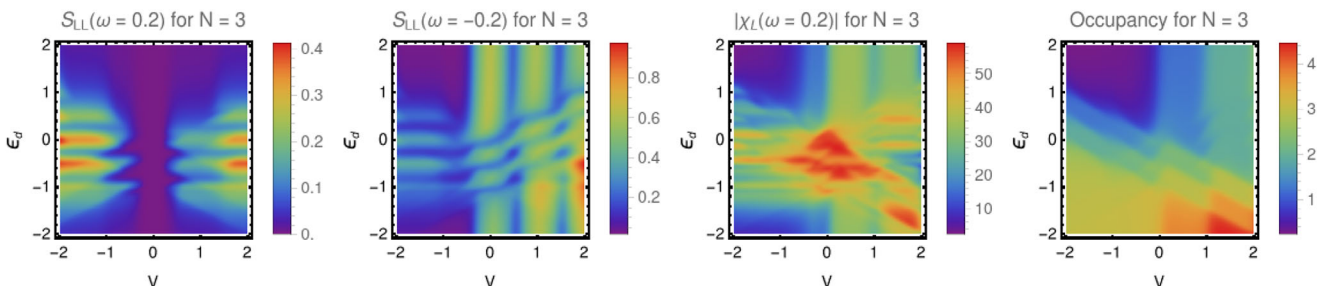


Figure 6. Same as in Figure 5 for $N = 3$. One takes $\epsilon_0 = 0.5$, ϵ_0 being the energy separation between the levels.

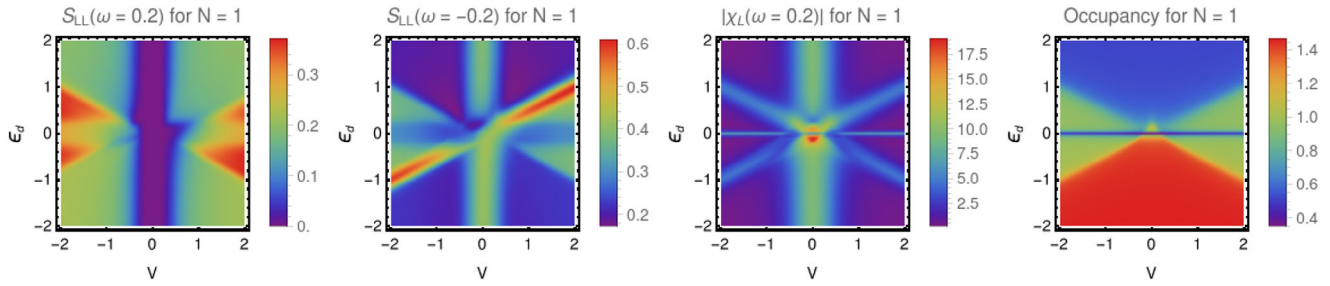


Figure 7. Color-scale plot for $S_{LL}(\omega)$, $|\chi_L(\omega)|$, and $\langle \hat{N} \rangle$ in a parallel-coupled DQD, as a function of bias voltage V and detuning energy ϵ_d at $|\omega| = 0.2$, $\Gamma_{L,R} = 0.1$, $\mathcal{V} = 0.1$, $\epsilon_1 = 0$, and $T = 0.01$, for one energy level in each dot ($N = 1$).

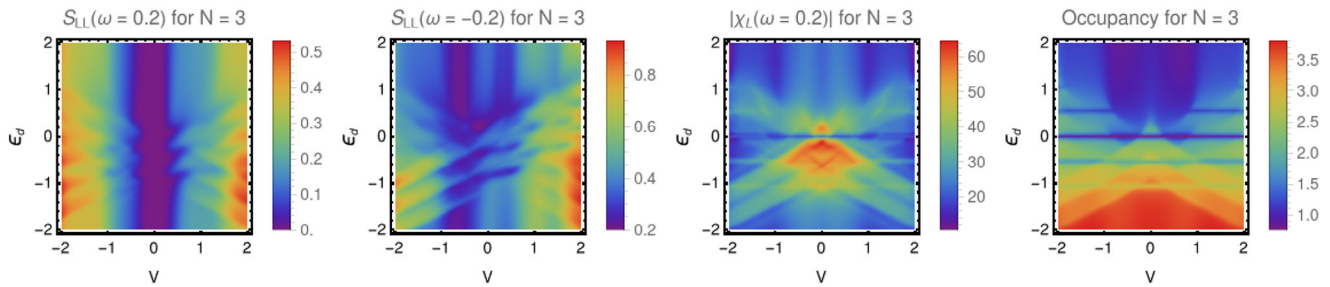


Figure 8. Same as in Figure 7 for $N = 3$. One takes $\epsilon_0 = 0.5$.

by equalling $\epsilon_2 + n\epsilon_0$ with $\epsilon_1 + m\epsilon_0$, where n and $m \in [0, N - 1]$. These horizontal lines are absent in the serial-coupled DQD case.

4.3. Side-Coupled DQD

Finally, **Figures 9 and 10** display the color-scale plots of the noise, the charge susceptibility and the dot occupancy as a function of

V and ϵ_d in a side-coupled DQD, as depicted on Figure 1e. The features present in the parallel-coupled DQD case for the charge susceptibility and dot occupancy, i.e. the existence of a vertical symmetry axis located at position $V = 0$ and the presence of horizontal lines at some specific positions of ϵ_d , are still there. However, one observes strong modifications in the variation profiles of absorption noise, and of charge susceptibility, with an

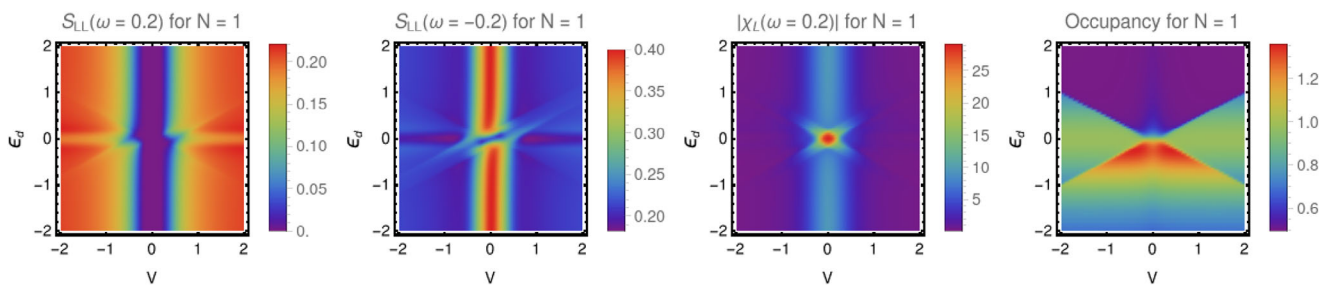


Figure 9. Color-scale plot for $S_{LL}(\omega)$, $|\chi_L(\omega)|$, and $\langle \hat{N} \rangle$ in a side-coupled DQD, as a function of bias voltage V and detuning energy ϵ_d at $|\omega| = 0.2$, $\Gamma_{L,R} = 0.1$, $\mathcal{V} = 0.1$, $\epsilon_1 = 0$, and $T = 0.01$, for one energy level in each dot ($N = 1$).

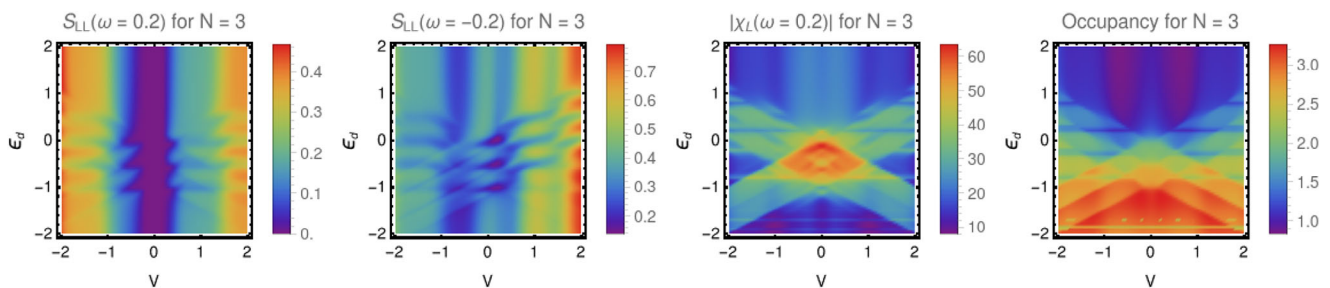


Figure 10. Same as in Figure 9 for $N = 3$. One takes $\epsilon_0 = 0.5$.

enhancement of their value within a vertical band of width $\hbar\omega$ centered around the line $eV = 0$. Even if for $N = 1$ the variation profiles of $S_{LL}(\omega)$, $\chi_L(\omega)$, and $\langle \hat{N} \rangle$ look very different when compared to the parallel-coupled and side-coupled DQDs, this is no longer the case when $N = 3$. Indeed these latter quantities show very similar variation profiles in this case (compare Figures 8 and 10). The reason for these similarities is related to the fact that when the dots contain several level of energies, the role played by the dot-reservoir coupling $\Gamma_{L,R}$ in the charge transmission through the DQD becomes less important compared to the role played by the dot-dot coupling \mathcal{V} , since the number of intra-processes are multiplied in the presence of multiple levels.

5. Conclusion

In this article, we have pointed out the similarities in the properties of finite-frequency noise and dynamical charge susceptibility in non-equilibrium quantum dot systems. We have formally established an explicit relationship between these two physical quantities in the case of single-level SQD. Such a simple relationship does not apply in multi-level SQD or DQD. However, studies on the variation of emission and absorption noises, dynamical charge susceptibility and dot occupancy with bias voltage and detuning energy, show similarities among them, that we have been able to characterize in various geometries. Experimental verification is now awaited, especially since finite-frequency noise and real/imaginary parts of the dynamical charge susceptibility are both measurable quantities.^[22,26–29] This work paves the way for further studies in order to examine whether these types of relationship are preserved in the presence of Coulomb interactions and spin degrees of freedom, which are known to play an important role in quantum dots systems. This remains to be done.

Conflict of Interest

The authors declare no conflict of interest.

Data Availability Statement

The data that support the findings of this study are available from the corresponding author upon reasonable request.

Keywords

dynamical charge susceptibility, finite-frequency noise, non-equilibrium Green functions, quantum dots

Received: July 28, 2023
Revised: September 19, 2023
Published online:

- [1] A. P. Vepsäläinen, A. H. Karamlou, J. L. Orrell, A. S. Dogra, B. Loer, F. Vasconcelos, D. K. Kim, A. J. Melville, B. M. Niedzielski, J. L. Yoder, S. Gustavsson, J. A. Formaggio, B. A. VanDevender, W. D. Oliver, *Nature* **2020**, 584, 551.

- [2] C. D. Wilen, S. Abdullah, N. A. Kurinsky, C. Stanford, L. Cardani, G. D'Imperio, C. Tomei, L. Faoro, L. B. Ioffe, C. H. Liu, A. Opremcak, B. G. Christensen, J. L. DuBois, R. McDermott, *Nature* **2021**, 594, 369.
- [3] B. Paquelet Wuetz, D. Degli Esposti, A. M. J. Zwerver, S. Amitonov, M. Botifoll, J. Arbiol, L. M. K. Vandersypen, M. Russ, G. Scappucci, *Nat. Commun.* **2023**, 14, 1385.
- [4] A. Crépeux, *Ann. Phys.* **2017**, 529, 1600344.
- [5] M. Prada, P. Harrison, *New J. Phys.* **2004**, 6, 30.
- [6] N. A. Zimbovskaya, *Phys. Rev. B* **2008**, 78, 035331.
- [7] M. Glässl, M. D. Croitoru, A. Vagov, V. M. Axt, T. Kuhn, *Phys. Rev. B* **2011**, 84, 125304.
- [8] A. Cottet, C. Mora, T. Kontos, *Phys. Rev. B* **2011**, 83, 121311.
- [9] R. Mizuta, R. M. Otxoa, A. C. Betz, M. F. Gonzalez-Zalba, *Phys. Rev. B* **2017**, 95, 045414.
- [10] L. E. Bruhat, T. Cubaynes, J. J. Viennot, M. C. Dartiailh, M. M. Desjardins, A. Cottet, T. Kontos, *Phys. Rev. B* **2018**, 98, 155313.
- [11] R. Aguado, L. P. Kouwenhoven, *Phys. Rev. Lett.* **2000**, 84, 1986.
- [12] R. López, R. Aguado, G. Platero, *Phys. Rev. B* **2004**, 69, 235305.
- [13] J. Aghassi, A. Thielmann, M. H. Hettler, G. Schön, *Phys. Rev. B* **2006**, 73, 195323.
- [14] N. Lambert, R. Aguado, T. Brandes, *Phys. Rev. B* **2007**, 75, 045340.
- [15] F. Bodoky, W. Belzig, C. Bruder, *Phys. Rev. B* **2008**, 77, 035302.
- [16] H.-F. Lü, J.-R. Zhang, T. Wu, Z. Xiao-Tao, H.-W. Zhang, *J. Appl. Phys.* **2010**, 107, 034314.
- [17] P. Shi, M. Hu, Y. Ying, J. Jin, *AIP Adv.* **2016**, 6, 095002.
- [18] N. Maslova, P. Arseyev, V. Mantsevich, *Sci. Rep.* **2021**, 11, 9336.
- [19] L. Tesser, M. Acciai, C. Spänslätt, J. Monsel, J. Splettstoesser, *Phys. Rev. B* **2023**, 107, 075409.
- [20] S. J. Chorley, J. Wabnig, Z. V. Penfold-Fitch, K. D. Petersson, J. Frake, C. G. Smith, M. R. Buitelaar, *Phys. Rev. Lett.* **2012**, 108, 036802.
- [21] J. J. Viennot, M. R. Delbecq, M. C. Dartiailh, A. Cottet, T. Kontos, *Phys. Rev. B* **2014**, 89, 165404.
- [22] R. Ezzouch, S. Zihlmann, V. P. Michal, J. Li, A. Aprá, B. Bertrand, L. Hutin, M. Vinet, M. Urdampilleta, T. Meunier, X. Jehl, Y.-M. Niquet, M. Sanquer, S. De Franceschi, R. Maurand, *Phys. Rev. Appl.* **2021**, 16, 034031.
- [23] R. Deblock, E. Onac, L. Gurevich, L. Kouwenhoven, *Science* **2003**, 301, 203.
- [24] R. Delagrange, J. Basset, H. Bouchiat, R. Deblock, *Phys. Rev. B* **2018**, 97, 041412.
- [25] K. Kobayashi, M. Hashisaka, *J. Phys. Soc. Jpn.* **2021**, 90, 102001.
- [26] D. T. McClure, L. DiCarlo, Y. Zhang, H.-A. Engel, C. M. Marcus, M. P. Hanson, A. C. Gossard, *Phys. Rev. Lett.* **2007**, 98, 056801.
- [27] S. Singh, J. T. Peltonen, I. M. Khaymovich, J. V. Koski, C. Flindt, J. P. Pekola, *Phys. Rev. B* **2016**, 94, 241407.
- [28] S. Singh, P. Menczel, D. S. Golubev, I. M. Khaymovich, J. T. Peltonen, C. Flindt, K. Saito, E. Roldán, J. P. Pekola, *Phys. Rev. Lett.* **2019**, 122, 230602.
- [29] S. Singh, E. Roldán, I. Neri, I. M. Khaymovich, D. S. Golubev, V. F. Maisi, J. T. Peltonen, F. Jülicher, J. P. Pekola, *Phys. Rev. B* **2019**, 99, 115422.
- [30] D. Y. Baines, T. Meunier, D. Maily, A. D. Wieck, C. Bäuerle, L. Saminadayar, P. S. Cornaglia, G. Usaj, C. A. Balseiro, D. Feinberg, *Phys. Rev. B* **2012**, 85, 195117.
- [31] J. A. Andrade, P. S. Cornaglia, A. A. Aligia, *Phys. Rev. B* **2014**, 89, 115110.
- [32] Y.-J. Wang, J.-H. Wei, *Chin. Phys. B* **2022**, 31, 097305.
- [33] M. Lavagna, V. Talbo, T. Q. Duong, A. Crépeux, *Phys. Rev. B* **2020**, 102, 115112.
- [34] A. Crépeux, M. Lavagna, *Phys. Rev. B* **2022**, 106, 115439.
- [35] R. Zamoum, M. Lavagna, A. Crépeux, *Phys. Rev. B* **2016**, 93, 235449.
- [36] A. Crépeux, S. Sahoo, T. Q. Duong, R. Zamoum, M. Lavagna, *Phys. Rev. Lett.* **2018**, 120, 107702.
- [37] A. Crépeux, T. Duong, M. Lavagna, *arXiv:2306.02146* **2023**.

- [38] G. Schull, N. Néel, P. Johansson, R. Berndt, *Phys. Rev. Lett.* **2009**, *102*, 057401.
- [39] F. Xu, C. Holmqvist, W. Belzig, *Phys. Rev. Lett.* **2014**, *113*, 066801.
- [40] M. Büttiker, A. Prêtre, H. Thomas, *Phys. Rev. Lett.* **1993**, *70*, 4114.
- [41] M. Filippone, K. Le Hur, C. Mora, *Phys. Rev. B* **2013**, *88*, 045302.
- [42] Y. Blanter, M. Büttiker, *Phys. Rep.* **2000**, *336*, 1.
- [43] J. Gabelli, G. Fève, J.-M. Berroir, B. Plaçais, A. Cavanna, E. B., Y. Jin, D. Glattli, *Science* **2006**, *313*, 499.